A Dinklage et al.

Magnetic configuration effects on the Wendelstein 7-X stellarator

En route to the demonstration of stellarator optimisation:
First magnetic configuration effects on Wendelstein 7-X plasmas

A. Dinklage[1,2], P. Helander[1,2], G. Fuchert[1], H. Maassberg[1], N. Marushchenko[1], K. Rahbarnia[1], T.Sunn Pedersen[1,2], Y. Turkin[1], R.C. Wolf[1,3], A. Alonso[4], T. Andreeva[1], C.D. Beidler[1], B. Blackwell[5], S. Bozhenkov[1], B. Buttenschön[1], A. Czarnecka[6], F. Effenberg[7], Y. Feng[1], J. Geiger[1], M. Hirsch[1], U. Hoefel[1], M. Jakubowski[1], T. Klinger[1,2], J. Knauer[1], G. Kocsis[8], A. Krämer-Flecken[9], M. Kubkowska[6], A. Langenberg[1], H.P. Laqua[1], A. Mollén[1], U. Neuner[1], H. Niemann[1], E. Pasch[1], N. Pablant[10], L. Rudischhauser[1], H.M. Smith[1], O. Schmitz[7], T. Stange[1], T. Szepesi[7], G. Weir[1], T. Windisch[1], G. Wurden[11], D. Zhang[1]
and the W 7-X Team

[1]Max-Planck-Institut für Plasmaphysik, Greifswald, Germany

[2]E.-M.-Arndt Universität Greifswald, Greifswald, Germany

[3]Technische Universität Berlin, Berlin, Germany

[4]CIEMAT, Madrid, Spain

[5]Australian National University, Canberra, Australia

[6]IPPLM, Warsaw, Poland

[7]U Wisconsin, Madison, WI, USA

[8]Wigner RCP RMI, Budapest, Hungary

[9]FZJ, Jülich, Germany

[10]PPPL, Princeton, NJ, USA

[11]LANL, Los Alamos, NM, USA

Abstract

At the end of 2015, the first plasma experiments were started in the Wendelstein 7-X (W7-X) stellarator. Based on an elaborate optimisation procedure, W7-X has been designed to achieve high-performance steady-state plasmas that extrapolate favourably to a future energy-producing fusion device. The optimisation includes the minimisation of spontaneously arising plasma currents and of the so-called neoclassical transport, which results from the complicated particle orbits in the three-dimensionally shaped magnetic field. Despite the technical limitations during the first experimental campaign, which preclude a comprehensive assessment of the optimisation properties, a number of promising results were achieved. The energy confinement time already shows values that are among the best ever obtained in stellarators. A set of experiments was performed to investigate the effect of the magnetic field characteristics on plasma confinement by varying the magnetic mirror ratio and the effective helical ripple ε_{eff} a commonly used figure of merit for the neoclassical transport in plasmas with a relatively weak radial electric field. In the experiments reported here, however, this field was very strong because of a peaked electron temperature profile, and the confinement times were, as a result, essentially independent of ε_{eff}. The optimisation of W7-X also sought to minimise the toroidal plasma (bootstrap) current, which was experimentally confirmed to be small and to respond as predicted to changes in the magnetic mirror ratio. Taken together, these initial experiments confirm several expected properties of W7-X plasmas, and already indicate that the observed results are consistent with optimisation measures.

Stellarator optimisation – a new opportunity for magnetic-confinement fusion?

The two leading concepts for confining high-temperature fusion plasmas are the tokamak and the stellarator [1]. Both use magnetic fields that follow helical paths and trace out toroidal magnetic flux surfaces in order to reduce the energy losses as far as possible. In tokamaks, the rotational transform, defined as the poloidal winding number of the magnetic field lines in one toroidal turn, is generated by a toroidal plasma current, while in stellarators three-dimensionally shaped coils are used for the same purpose. As a result, the magnetic-field geometry of the two concepts is fundamentally different. In the tokamak, the magnetic field strength B varies from the inside of the torus to the outside, but is constant in the toroidal direction. (Toroidal refers to the long way around the torus, poloidal to the short way.) This toroidal symmetry results in the conservation of the (canonical) angular momentum of each particle, which implies that collisionless particle trajectories are confined within the plasma. A hot fusion plasma is of course not collisionless –collisions are required to produce fusion reactions – but the collision frequency is so low that the confinement is very poor unless most collisionless orbits are well confined. In contrast to tokamaks, stellarators lack toroidal symmetry and have a truly 3-dimensional magnetic field [2]. As a result, particles trapped in magnetic mirrors (local minima of the field strength) along the field can drift out of the plasma confinement region. Already half a century ago, it was recognised that the collisional transport is strongly affected by the geometry of the collisionless orbits [3]. While in tokamaks this so-called neoclassical transport is usually unimportant compared with the energy loss caused by plasma turbulence, the neoclassical transport losses in stellarators can become very large at high plasma temperature T and for the fast α-particles produced in deuterium-tritium fusion reactions. The transport coefficients in stellarators depend sensitively on the collision frequency ν as well as the drift velocity $v_D \sim mv^2/(2qRB)$ (where v denotes the speed, m the mass and q the charge of the particles in question and R is the major radius of the device) and the radial electric field E_r across the magnetic surfaces. When the latter is small and the mean free path between collisions is long, the transport coefficient for electron heat conduction across the magnetic surfaces usually scales as $D^{1/\nu} \sim \varepsilon_{eff}^{3/2} v_D^2/\nu \sim T^{7/2}$, resulting in a heat flux proportional to $T^{9/2}$. (Strictly speaking, it is the so-called mono-energetic radial transport coefficient that scales this way. It refers to the transport of particles with a definite energy, whereas the total transport is obtained by an appropriate average over the energy distribution of all particles.) The effective helical ripple, ε_{eff}, characterises the transport due to the deviation of the magnetic geometry from perfect symmetry and is so large in classical (un-optimised) stellarators that the energy losses become prohibitively high at temperatures required for a burning fusion plasma. The neoclassical transport can be moderated by the electric field, which acts to confine the drift motion of the plasma particles and results in a modified scaling of the radial transportas $D^{\sqrt{\nu}} \sim v_D^2 E_r^{-3/2} \sqrt{\nu} \sim T^{5/4} E_r^{-3/2}$ depending, as it were, more favourably on the collision frequency and temperature. These transport regimes are peculiar to stellarators. A further difference from tokamaks is that the neoclassical transport is not ``intrinsically ambipolar'': The electron and ion particle fluxes are in general not equal, and they depend differently on the electric field. E_r therefore adjusts to whatever value is required to keep the electron and ion charge fluxes opposite and equal so that the plasma can reach a steady state without further charge accumulation. The resulting equation for E_r is nonlinear and can have several solutions (roots) which themselves depend on the local plasma parameters. When the density is high, due to thermalization the electron and ion temperatures approach each other, and the so-called ion root appears. Here the radial electric field points towards the plasma center. At lower densities, the electron temperature is often

significantly higher than the ion temperature and the electric field reverses sign; here one speaks of the electron root [4].

At temperatures and densities required to achieve a burning deuterium-tritium plasma ($10 - 20$ keV and ~10^{20} m^{-3}), stellarator plasmas are generally expected to be in the ion-root transport regime. The corresponding inward electric field reduces the ion fluxes (in the $\sqrt{\nu}$ transport regime) to match the electron flux (in the $1/\nu$ transport regime) [5]. The resulting high neoclassical $1/\nu$ transport with its unfavourable temperature dependence was for a long time considered to be a show-stopper for stellarators. A way to mitigate drift-enhanced losses was proposed by Palumbo [6]. He argued that the magnetic field could be tailored in such a way that magnetic drifts across the flux surfaces vanish everywhere. He called such fields isodynamic. Full isodynamicity, however, cannot be achieved in toroidal geometry, but it was later realised that the average drift could be made to vanish for a sufficiently large majority of the orbits such that net fusion energy production is possible. A systematic exploration of magnetic configurations has revealed quasi-isodynamic configurations where trapped particles follow poloidally closed orbits and do not drift out of the plasma [7]. This property leads to a significant reduction of radial drifts and therefore a reduction of the α-particle losses and of $1/\nu$ transport of the thermal plasma if compared to a non-optimized, classical stellarator.

To really find a stellarator configuration that fulfils the basic requirements of confining and sustaining a high-temperature fusion plasma for a considerable amount of time (of the order of an hour), much more than the neoclassical confinement has to be considered. With the advent of powerful computers it has become possible – using numerical optimisation algorithms - to find magnetic field configurations which simultaneously fulfil a number of requirements, including low neoclassical transport, sufficient plasma stability at volume averaged β-values (ratio between plasma pressure and magnetic field pressure) up to 5%, and a workable exhaust concept for removing heat and particles from the plasma. The magnetic field has to be generated by shaped (possibly superconducting) magnetic field coils and it is another requirement that they can be constructed and assembled without too much difficulty. The type of configuration resulting from this optimisation procedure for W7-X was termed the helical-axis advanced stellarator (in short HELIAS) [8]. The stellarator W7-X is thus the first of the HELIAS line.

One fundamental property of the HELIAS configuration is the minimisation of electric plasma currents. Self-generated plasma currents always occur in magnetised plasmas, and these currents modify the magnetic field. The HELIAS concept seeks to minimise the effect of plasma currents on the designed confining magnetic field. Self-generated currents are the bootstrap current, the Pfirsch-Schlüter currents and the diamagnetic current. The bootstrap current is a net toroidal current driven by the pressure gradient [9,10]. It originates from the fact that the particle orbits are such that there is a correlation between the parallel (to B) velocity and the radial position of trapped particles. For instance, in a tokamak the trapped ions move in the direction of the plasma current on the outboard leg of their (banana) orbit and in the opposite direction on the inboard leg. The opposite is true for the electrons, so if there is a pressure gradient across a given magnetic surface, the number of co-current-moving particles of either species is different from that of the counter-moving ones, and a net current therefore arises. Something similar happens in stellarators, but the relation between parallel velocity and radial position along particle orbits is different, and so is therefore the bootstrap current. It can flow in either direction, and W7-X has been optimized to make it as small as possible.

The bootstrap current has been observed experimentally both in tokamaks [11] and stellarators [12] and agrees broadly with theoretical expectations.

Ideal isodynamicity implies that the bootstrap current vanishes [13,14], but isodynamicity in W7-X is only approximate. Therefore, the bootstrap current does not vanish exactly and does not reach its lowest value in the magnetic configurations that have the lowest neoclassical transport, but it is nevertheless much smaller than in a typical tokamak. Isodynamicity is most closely realised in the core of the plasma when the pressure profile is steep enough. Going from the plasma edge to the centre, the rotational transform ι decreases only slightly and the magnetic shear $d\iota/dr$ is low. This means ι can be chosen in such a way that resonances corresponding to low-order rational values of ι are avoided in the confinement region. Such resonances usually lead to a loss of confinement by the formation of magnetic islands. If ι is chosen close to unity value at the plasma edge, the resulting magnetic islands can be used to divert the edge plasma to specially designed target plates. Since the formation and position of those islands sensitively depend on the precise value of ι, even small plasma currents need to be controlled. In addition, small magnetic shear is used to generate magnetic islands wide enough for feasible heat and particle exhaust.

The required, carefully tailored magnetic field of a HELIAS is created by a set of shaped magnetic field coils. Fig. 1 shows the main components of the W7-X device. 50 modular, non-planar coils generate the confining magnetic field. 20 planar coils can be used to adjust the rotational transform and change the radial position of the plasma. The coils are superconducting (Niobium-Titanium) to allow for steady-state plasma operation. The magnetic field has five-fold symmetry and forms five linked magnetic mirrors.
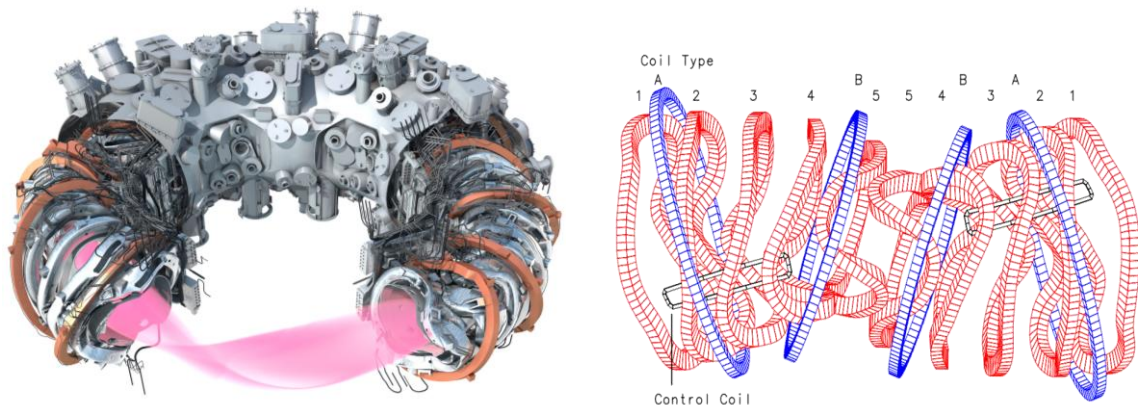
Fig. 1: Left: Schematic CAD drawing of Wendelstein 7-X (© IPP). Going from the inside to the outside the main components are: Plasma, vacuum vessel, field coils, (planar coils: copper, non-planar coils silver) coils support structure, cryostat vessel with (254) ports providing access to the plasma vessel. The torus has a mean diameter of 11 m and a mean minor radius of about 0.55 m leading to plasma volumes of about 30 m^3. Right: Arrangement of non-planar, modular coils (red), planar coils (blue, coil type A is close to the pentagon corners, coil type B acts on the straight section of the module) and control coils (black) in one (of five) module of W7-X. The coil types are labeled and their arrangement reflects the specific stellarator symmetry.

Elements of the coil design were already tested on the predecessor experiment of W7-X, Wendelstein 7-AS [15]. The modular [16], non-planar coils are shaped in such a way that the resulting field geometry meets the different optimization requirements. In particular at higher magnetic fields,

special care has to be taken to accommodate the mechanical shear forces produced by the charged coils. In addition, the coils have to be precisely manufactured and assembled to avoid perturbations of the magnetic field topology. It has been demonstrated that W7-X possesses nested magnetic flux surfaces with measured relative field errors $\delta B/B$ smaller than 10^{-5} [17].

Here, we present results from the first experimental campaign of W7-X, which lasted from December 2015 until March 2016. In this phase, the heat was taken by five un-cooled graphite limiters designed to follow the expected shape of the last closed flux surface [18]. In order to keep the temperature rise on the limiter surfaces well below the sublimation temperature of graphite, the maximum energy delivered to the plasma during a single pulse was set to 4 MJ. Even at minimum power levels required to sustain plasmas (~ 0.6 MW), all discharges were much too short to reach a stationary plasma equilibrium. This requires plasma currents to saturate which only happens on the time scale given by the ratio of plasma inductance L to the plasma resistance R. Even for the longest pulses (~6s), the related L/R-time $\tau_{L/R} \sim 20\ s$ is much longer than the plasma lifetime.

The main objective of the campaign was the integral commissioning of the device, including first plasma generation, plasma-vessel conditioning, and the successive commissioning of about 30 plasma diagnostics [19]. Thanks to careful preparation, the commissioning phase could be conducted without major problems and about half of the time was used for physics studies, which despite the brevity of the campaign, lead to a wealth of results [20,21,22]. Plasma experiments were limited to relatively low plasma density, thus precluding high plasma pressure and access to the $1/\nu$ regime for which the magnetic field was mainly optimised. This is, however, well in line with the chosen staged approach to steady-state operation in relevant collisionality regimes at high heating power [23].

In this paper we report first detailed assessment of neoclassical physics in W7-X. Initial conclusions on the efficacy of the optimisation and other fundamental properties of the HELIAS are drawn.
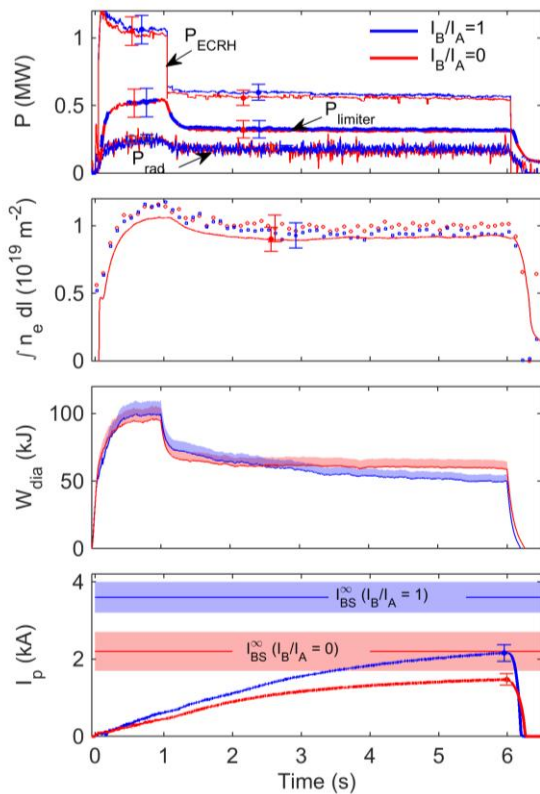

Fig. 2: (From top to bottom) Time traces of (a) heating power and power losses, (b) plasma line density, (c) diamagnetic energy and (d) plasma currents comparing 'lower mirror' (blue, $I_B/I_A = 1$) and the 'higher mirror' (red, $I_B/I_A = 0$) magnetic field configurations. Uncertainties are representative for the entire waveform (cf. methods section).

Effect of magnetic field variations on perpendicular and parallel transport

A key question of the first operation campaign was if single aspects of the W7-X optimization could already be tested, given the limited capabilities of the device for that campaign (e.g. limited heating power, density, pulse length, plasma pressure). To test the effect of the magnetic field geometry on heat transport
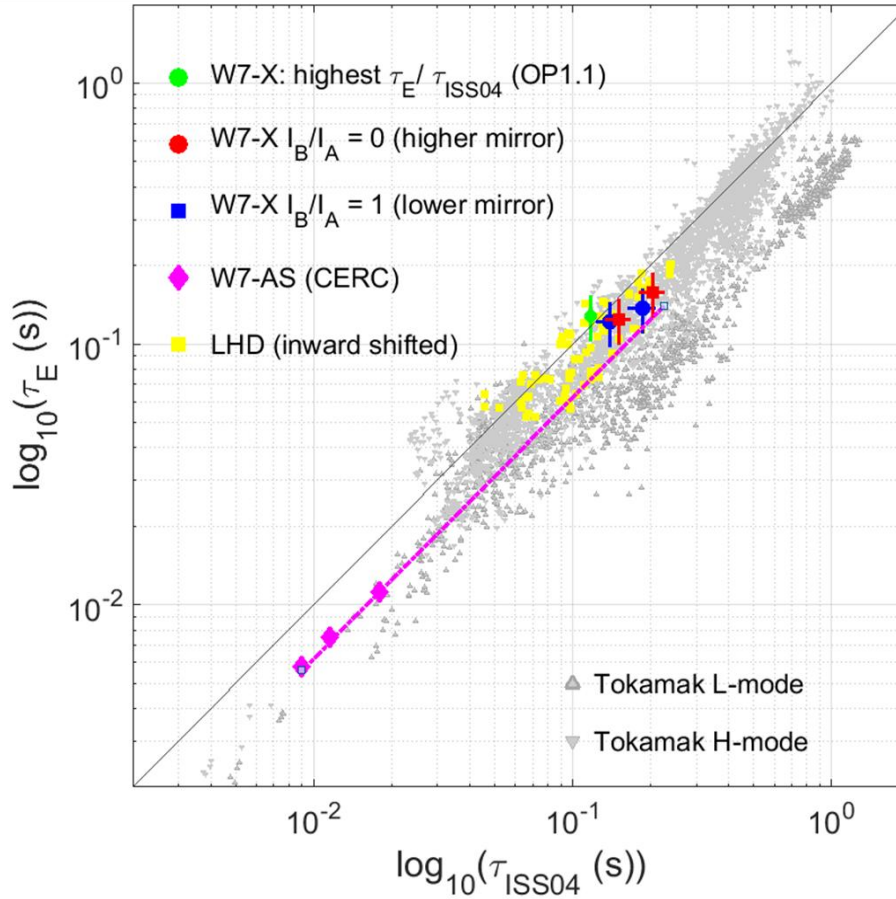
Fig. 3: Energy confinement times τ_E vs scaling expectations τ_{ISS04}. W7-X data refer to cases discussed in this paper and the discharge with the highest confinement enhancement in the first experiment phase. Tokamak data are rephrased in terms of the stellarator confinement scaling. Confinement data from CERC discharges on W7-AS. The magenta line indicates the scaling expectation from these W7-AS data extrapolated to W7-X parameters.

and plasma currents, two configurations with different magnetic mirror ratios were compared. Changes were made by adjusting the ratio of the currents in the planar coils of type A and B (cf. Fig. 1(b)) which alters the depth of the toroidal magnetic mirror. The corresponding mirror ratio is given by the maximum and minimum field strengths along the magnetic axis as $(B_{\max} - B_{\min})/(B_{\max} + B_{\min})$. $I_B/I_A = 0$ causes the magnetic induction in the straight sections of the pentagon to be reduced and thus gives a 'higher-mirror' configuration (red lines throughout this paper, mirror ratio 6.0%, see also Fig. 5(b) in the Methods section). The current ratio $I_B/I_A = 1$ results in a 'lower-mirror' configuration (blue lines, mirror ratio 3.7%). The change in the coil current directly affects the particle orbits and thus the characteristics of the neoclassical transport.

The variations of the coil current ratios of the planar coils have only a small effect on the rotational transform. Note that the small increase of the rotational transform leads to an inward shift of the island chain, corresponding to an inward shift of the position of the resonance at $\iota = 5/6$ (see also Fig. 5(b) in the Methods section). As mentioned above, at low collisionalities the optimisation parameter ε_{eff} has an effect on the $1/\nu$ plasma transport. The effective helical ripple of the lower-mirror case is about half of the ripple for the higher-mirror case (see also Fig. 5(c) in the Methods section). The effect of magnetic mirror change on the plasma parameters is shown in Fig. 2. For both configurations, the heating power was set to 1.0 MW for one second and lowered to about 0.6MW

7

for the remaining 5 s. Given the technical energy limit of 4 MJ, these settings allowed for a total pulse length of 6 s. Power losses by radiation P_{rad} and convective heat losses onto the limiters $P_{limiter}$ add up to more than 80% of the total heating power (Fig. 2(a)) [24]. The remaining 20% presumably leave the plasma by charge-exchange processes with neutrals that are released by the plasma-facing components and may also involve errors in the measurements (discussed in the methods section). The power traces in the higher- and lower-mirror cases are nearly identical, indicating that the power-loss mechanisms are similar. The plasma line density (Fig. 2(b)) is stationary after a few hundred ms and stays constant. Since no additional gas fuelling was applied, the stationary density indicates full recycling of plasma particles. Such stationary plasma densities required dedicated glow-discharge-cleaning of the in-vessel components. The confinement quality is represented by the temporal evolution of the plasma diamagnetic energy [25,26], which remains constant or slightly decays during phases of constant heating power (note that energy confinement time $\tau_E = W/P$; W stored plasma thermal energy, P: heating power).

Fig. 3 shows τ_E for the discharges discussed in this paper plotted against scaling expectations (ISS04 scaling [27]). The figure also contains the W7-X discharge with highest $\tau_E/\tau_{ISS04.}$ [(128±25)ms/117ms] The W7-X data are displayed with results from LHD (inward shifted configuration with best confinement) [27] And the energy confinement times of early W7-X discharges are among the highest attained in helical devicesA comparison with similar discharge conditions in the (partly optimized) predecessor device Wendelstein 7-AS already indicates significant improvement in the confinement in terms of the confinement factor τ_{exp}/τ_{ISS04} which takes differences in geometry, heating power and density into account (seen as an increase with respect to the magenta line in Fig. 3). While W7-X is too small to operate at fusion reactor conditions, the present findings can be compared to tokamak discharges by expressing the empirical stellarator confinement scaling ISS04 [27] in terms of tokamak parameters [28, 29] [29]. The data derived for the discharge presented here indicate that the energy confinement time of W7-X limiter plasmas [30] is well in the range of tokamak high-confinement (H-mode) plasmas (cf. Fig. 3), which is the reference for achieving a burning fusion plasma in ITER ($P_{fusion}/P_{heating}$ = 10) [31].

While the global confinement is less affected by changes in the mirror ratio than expected from $1/\nu$ heat transport, the toroidal plasma current responds quite sensitively to changes in the magnetic field (cf .Fig. 2(d)). The measurements show after 6 s rising but saturating plasma currents. At the end of the discharge the plasma current in the lower-mirror case is 2.15 kA and in the higher-mirror case 1.47 kA, respectively. These values, much smaller than currents expected for current control [32], confirm an important aspect of the W7-X optimisation which is the minimization of the absolute value of the bootstrap current. The toroidal current needs to be small, otherwise the location of the island will move during the discharge if not controlled by, e.g. additional current drive [32]. Also shown in the diagram (Fig. 2(d)) are the respective stationary bootstrap currents I_{BS}^{∞} (with error bands), derived with neoclassical theory using measurements of temperature and density profiles. The toroidal current is still far from saturated (the predicted saturation time is about 20 seconds for these discharges), but they extrapolate well to those predicted from theoretical calculations for the steady state. The ratio of measured currents at the end of the plasma at t=6 s ($I_{higher\ mirror}/I_{lower\ mirror}$ = (1.47±0.15)kA/(2.15±0.22)kA = 0.69±0.10) shows good agreement with the ratio of the calculated stationary bootstrap current values ($I_{BS\text{-}higher\ mirror}^{\infty}/I_{BS\text{-}lower\ mirror}^{\infty}$ = 0.61±0.15). Thus, our measurements match the expectations closely. A numerical calculation of an equivalent tokamak discharge with the same profiles shows a factor of 3.5 larger bootstrap current, clearly inconsistent

with our measurements. More details of the numerical calculations and the bootstrap minimization strategy are given in the Methods section. If the plasma had lasted longer than several $\tau_{L/R}$ times and the toroidal plasma current would have reached I_{BS}^{∞} that would have indicated that the neoclassical bootstrap current would have been consistent with the saturated plasma currents.

Since I_{BS}^{∞} in the neoclassical picture only depends on the magnetic field configuration if the thermodynamic forces ($\nabla T_{e,i}/T_{e,i}$, $\nabla n/n$, E_r) are kept constant (as is the case in the experiments presented here), the observation clearly matches the expectation.

(a)

(b)
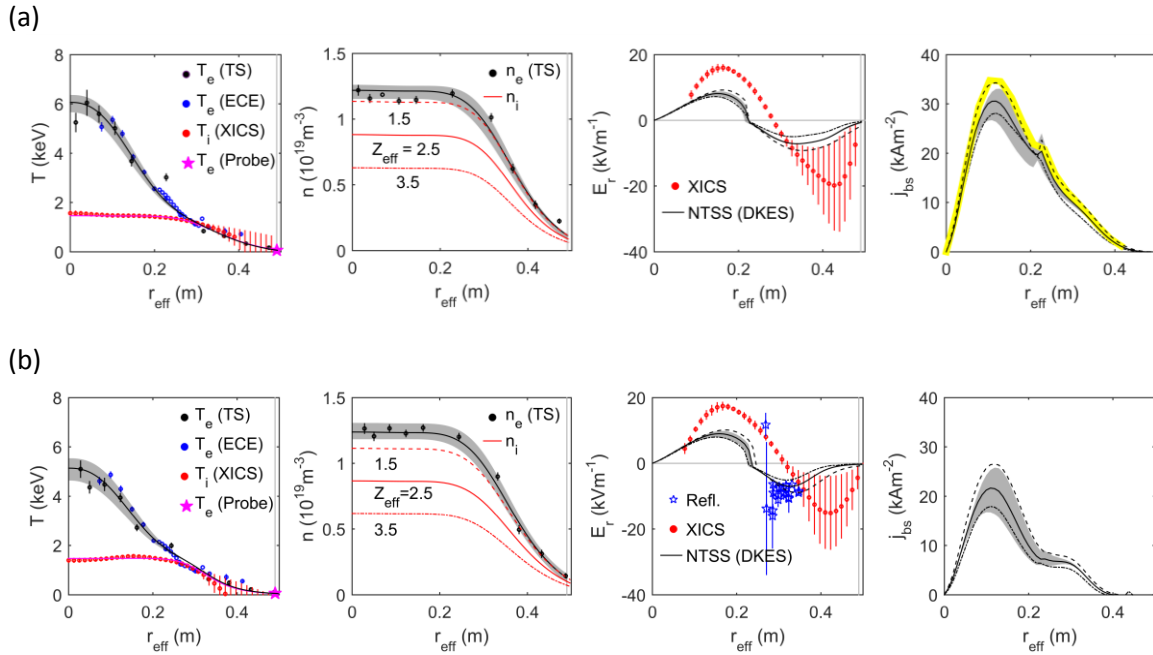
Fig. 4: Plasma profiles for the lower-mirror (a) and higher-mirror (b) magnetic configuration during the initial heating phase (t = 0.7s in Fig. 2). The radial electric field profile (third column) measurements (using X-ray imaging spectroscopy, XICS, and reflectometry) are compared to neoclassical modeling with fits to the profiles of plasma temperatures and densities (first and second column) assuming spatially constant Z_{eff}-values. Grey shaded areas indicate uncertainties of the profile measurements. Due to the uncertainties of the experimentally estimated Z_{eff}-values, Z_{eff} variations from Z_{eff} = 1.5 … 3.5 have been assumed. All throughout this paper, corresponding uncertainties follow the line code in the density profile plot. The assumed impurity species was carbon. The fourth column shows the calculated neoclassical bootstrap current density profiles, the yellow line shows results from SFINCS calculations (cf. Methods section).

Fig. 4 shows the measured temperature and density profiles as well as profiles of the radial electric field and the predicted bootstrap current density (derived from the pressure profiles) at t= 0.7s. In this phase, measurements of the radial electric field were available which allow one to compare between calculations and measurements of E_r. For both the lower- and higher-mirror configuration cases, temperature and density profiles are similar for the two configurations. Using fits to the experimental data, particle and energy fluxes were also calculated and used to compute the expected radial electric field using the NTSS code [33]. The result is compared to direct measurements of E_r using X-ray imaging spectroscopy [34] and correlation reflectometry [35]. Both the measured and calculated E_r-profiles indicate a strong positive radial electric field in the plasma core. Towards the plasma edge E_r becomes negative, which can be seen as evidence for a spatial bifurcation of the neoclassical transport from core electron-root confinement ($E_r > 0$) in the plasma

centre to ion-root confinement more towards the edge ($E_r < 0$) [4]. The observation of core electron root confinement is supported by the fact that the central electron temperature has a peaked profile and is much higher than the ion temperatures.

These results explain why the change in ε_{eff} from the lower- to the higher-mirror configuration does not affect the energy confinement: Because of the large radial electric field, even the electrons are in the $\sqrt{\nu}$ transport regime in the plasma centre, and in the more peripheral regions the plasma becomes too collisional. The neoclassical radial transport is therefore only marginally affected by the change of the magnetic field configuration since the heat diffusivity is largely affected by the radial electric field. Therefore, the change of ε_{eff} by a factor of about two only plays a minor role for the experiments reported here. Moreover, anomalous contributions, acting predominantly in colder plasma regions, are expected to be much less affected by configuration changes as well.

Summary

The first experimental campaign of W7-X was successful and all major goals were achieved or even exceeded (e.g. pulse length, and achieved electron and ion temperatures). About 30 diagnostic systems were taken into operation, as was the ECR heating system, which proved to be both reliable and flexible. This made it possible to conduct a first physics program

The energy confinement time of the reported discharges has shown virtually no change when the magnetic configuration is changed, which is in line with the expected resilience of confinement against magnetic ripple in the core-electron-root confinement regime that is characteristic for the presented discharges. The bootstrap current could be confirmed to be substantially lower than that in tokamaks and its dependence on the mirror ratio was found to agree qualitatively with neoclassical theory. These findings provide an important confirmation of one of the key elements of the W7-X optimization; i.e. the minimization of the bootstrap current.

In future campaigns, significantly higher performance, and a much more comprehensive exploration of the parameter space will be possible. This will allow more detailed studies and a systematic verification of the W7-X optimisation.
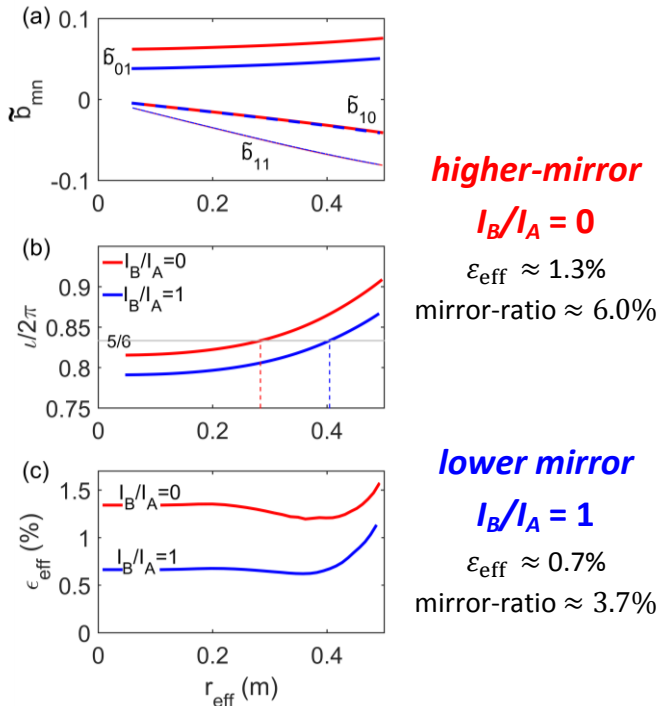
Acknowledgements

Methods

Plasma generation: For a description of the technical operation of the device W7-X see Ref. [36]. Plasma heating was conducted with electron cyclotron resonance heating (ECRH) equipped with specific protective diagnostics [37]. The heating power was measured with microwave diodes calibrated with calorimetry and stray-radiation was measured to be small for the applied X2 heating [38] resulting in uncertainties if the heating power of +5%/-10%. The working gas (hydrogen) was injected prior the discharge. The plasma facing components were conditioned by glow discharge cleaning before both experiments.

Magnetic configuration changes and actors for bootstrap current minimization: The change in the magnetic configuration was made by changing the operation current in planar coil type B while readjusting the coil current ratios for all other coils to keep the ECRH resonance condition, i.e. to adjust B to 2.5 T in the corner section of the W7-X pentagon. The specific effect on parameters that quantitatively affect the bootstrap current lies in the leading harmonics $\tilde{b}_{mn}$ of the Fourier representation of the magnetic field

$$(B/B_0 = \sum \tilde{b}_{mn}(cos(m\theta - nN\varphi))$$

with m, n the poloidal and toroidal mode numbers, $N = 5$ the number of field periods and θ, φ the poloidal and toroidal angles, respectively. Fig. 5 shows radial profiles of key quantities characterizing the configurations. The Fourier harmonics directly enter into the neoclassical transport coefficients [39,40]. In the experiments described here, both the toroidal curvature term $\tilde{b}_{10}$ and the helical component of the magnetic field $\tilde{b}_{11}$ are almost unaffected by the change

higher-mirror

$I_B/I_A = 0$

$\varepsilon_{\text{eff}} \approx 1.3\%$

mirror-ratio $\approx 6.0\%$

lower mirror

$I_B/I_A = 1$

$\varepsilon_{\text{eff}} \approx 0.7\%$

mirror-ratio $\approx 3.7\%$

Fig. 5: Radial profiles of important magnetic field properties. (a) – (c) show spatial variations (along the minor radius of the plasma cross-section r_{eff}) of characteristic quantities describing the magnetic field properties. (a) the leading Fourier components $\tilde{b}_{mn}$ (b) $\ell = \iota/2\pi$ (rotational transform) and (c) ε_{eff} (the effective helical ripple).

of I_B/I_A. Fig. 5(a) illustrates the main effect in the Fourier components of the field to be an increase of the toroidal mirror term $\tilde{b}_{01}$ (here the most contributing Fourier component to the magnetic mirror ratio) when the current in the planar coils of type B is lowered.

Numerics: The properties of the magnetic field geometry were calculated with the MHD equilibrium code VMEC [41]. Vacuum field calculations have been conducted with a field-line tracer code [42]. The neoclassical transport analyses (E_r and j_{BS} calculations) were conducted with the NTSS code which employed neoclassical transport coefficients from the DKES code [43,44]. The NTSS code and dedicated DKES calculations were also used to conduct calculations for an equivalent tokamak. The SFINCS code [45] with an extended neoclassical model (not relying on the assumption

of incompressible ExB drifts and using a full inter-species linearized Fokker-Planck operator) was employed for model comparison resulting in about 10% higher bootstrap current than NTSS for the cases discussed in this paper. For both power deposition calculations and electron cyclotron current drive calculations, the electron cyclotron ray tracing code TRAVIS [46] was used.

Data validation: For the overall power balance, the heat load patterns on the limiter were validated with plasma edge simulations with the EMC3-EIRENE [47] code. Measurements of the heat flux patterns on the limiters for the two configurations investigated, which formed the boundary between confinement region with closed magnetic field lines and the scrape-off layer with open field lines, showed that changes in these patterns can be explained by variations in the connections lengths of the magnetic field lines in the scrape-off layer [48].

Plasma diagnostics: An overview on W7-X diagnostics is given in Ref. (i.e. $E_r > 0$ for $r_{eff}/a < 1/2$)]. The radiated power profile was derived by Abel-inversion of measurements from a bolometer array. The inversion does not take asymmetries into account. Overall uncertainties for the radiated power are around 10%. The line density was measured with a dispersion interferometer at relative errors of less than 10%. Line densities from Thomson data were derived from density profiles mapped with VMEC equilibrium calculations on the line of sight of the interferometer. Uncertainties in Fig. 2(b) mainly result from the scatter of Thomson data and measurement errors in the observation channels propagating to relative uncertainties of 10% in the line integral derived from Thomson scattering data. The error the plasma current measurements with the Rogowski coils is about 10% [26]. The density profiles were measured by Thomson scattering. Spatially resolved electron temperature measurements were conducted with electron cyclotron radiometry and Thomson scattering. Electron temperatures at the last closed flux surface position were determined from Langmuir-probe measurements. Measurements of line averaged Z_{eff} values were derived from the Bremsstrahlung contribution in pulse height analysis spectra resulting in $Z_{eff} = 2.5 \pm 1$. Ion temperature profiles were derived from a tomographic inversion of X-ray imaging spectroscopy as well as poloidal plasma velocity measurements. The associated errors reflect both the inversion and the radial dependent signal to noise ratio of the X-ray emissivity [50]. The diamagnetic energy measurements had systematic offsets of 8% (included in (cf. Fig. 2)) and scatter in comparison with the kinetic energy around 10%. The kinetic energy had a total error of 20% as reflected by the error bars in Fig. 3. Poloidal velocities were also derived from correlation reflectometry with errors considering the correlation procedure [35]. The plasma volume was cross-checked with video camera images. The power deposition profile was checked with heat-wave correlation measurements (ECE) in separate experiments at the same magnetic configuration.

Heat Flux Modeling: Complementing the modeling results in Fig. 4, Fig. 6 shows neoclassical heat fluxes Q_{NC} calculated from measured plasma profiles with NTSS. Q_{NC} is compared to the heating power P_{ECRH} with substracted radiated power (from Abel inversion). The spatial variation of P_{ECRH} was determined from deposition calculations with the TRAVIS code. Errors are due to the measured ECRH
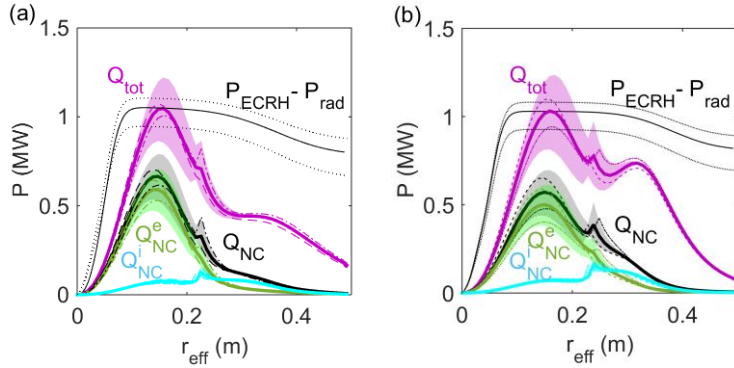
Fig. 6: Profiles of integrated heating power and transport losses (P_{ECRH}, P_{rad}, dotted lines show error bands) in comparison to modeled heat fluxes Q. Figures (a – lower mirror) and (b – higher mirror) correspond to Figs. 4(a) and (b) respectively. The neoclassical heat fluxes Q_{NC} is calculated with DKES transport coefficients without additional assumptions. The anomalous contribution to the total heat fluxes has free parameters. Patches correspond to uncertainties in the profiles, lines to Z_{eff} uncertainties. The heating uncertainties comprise uncertainties in the measurement of the heating power and bolometer measurements.

power and bolometer measurements. The TRAVIS calculations deliver also the electron cyclotron current confirming earlier estimates of almost negligible current drive [51] (for the lower mirror case I_{ECCD}^{∞} = (54 ± 25) A and for the higher mirror case I_{ECCD}^{∞} = (60 ± 25) A with errors due to profile and Z_{eff} uncertainties). Q_{NC} from the NTSS code corresponds up to (63±12)% (lower mirror) and (55±15)% (higher mirror) of the deposited power in the core region (i.e. E_r >0 for r_{eff}/a < ½, a is the minor plasma radius). The remaining heat flux is modeled with a phenomenological model χ^e_{ano} ~ 1/n. In order to match the total heat flux Q_{tot} = Q_{NC} + Q_{ano} with P_{ECRH}-P_{rad} in the plasma core (r_{eff}/a ~ 1/3), an anomalous heat diffusivity of χ_{ano}^e = (0.24±0.06) m^{2}s^{-1} is required to model the heat flux (Fig.6). For r_{eff}/a > 1/2, however, the phenomenogical model fails and the modeled heat fluxes are significantly lower than P_{ECRH}-P_{rad}. This remains true if the anomalous ion heat fluxes are included and chosen such that the ion heat flux does not exceed the electro-ion collisional transfer power. This choice overestimates the ion heat diffusivity since additional ion energy losses by charge exchange losses are not considered.

With these assumptions, the heat fluxes can be modeled as neoclassical heat transport (with dominant $\sqrt{\nu}$ contribution) and anomalous electron heat transport in the core region. Outside the core region, neoclassical heat fluxes are insufficient to describe the heat fluxes. No phenomenological model available in NTSS could be found to consistently model the remaining heat flux for r_{eff}/a > ½. The neoclassical heat flux and the anomalous heat flux in the two cases of magnetic mirrors do not vary with $\varepsilon_{eff}^{3/2}$ (as for neoclassical 1/ν transport).

Data availability. The data that support the plots within this paper and other findings of this study are available from the corresponding author upon reasonable request.

Author Contributions

AD, PH, TSP, RCW and TK wrote the paper. AD, TSP, SB, FE and JG prepared the configuration changes and the discharge program. AD, HM, YT, TA, AA, CDB, FE, YF, JG, AM, NM, HMS and OS did modeling

and data validation. KR, BB, BB, AC, GF, MH, UH, MJ, JK, GK, AKF, MK, AL, HL, UN, HN, EP, NP, LR, TS, TS, GW, TW, GW and DZ did measurements and data analysis.

Competing financial interests

References

[1] L. Spitzer, Project Matterhorn Report PM-S-1 NYO-993, Princeton University (1951) and The Stellarator Concept , Phys. Fluids **1**, 253 (1958)

[2] P. Helander, C.D. Beidler, T.M. Bird, M. Drevlak, Y. Feng, R. Hatzky, F. Jenko, R. Kleiber, J.H.E. Proll, Yu. Turkin and P. Xanthopoulos, Stellarator and tokamak plasmas: a comparison, Plasma Phys. Contr. Fusion **54**, 124009 (2012)

[3] A. A. Galeev, R. Z. Sagdeev, H. P. Furth and M. N. Rosenbluth, Plasma Diffusion in a Toroidal Stellarator, Phys. Rev. Lett. **22**, 511 (1969)

[4] M. Yokoyama, H. Maaßberg, C.D. Beidler, V. Tribaldos, K. Ida, T. Estrada, F. Castejon, A. Fujisawa, T. Minami, T. Shimozuma, Y. Takeiri, A. Dinklage, S. Murakami and H. Yamada, Core electron-root confinement (CERC) in helical plasmas, Nucl. Fusion **47**, 1213 (2007)

[5] A.A. Galeev and R.Z. Sagdeev, Theory of neoclassical diffusion, Reviews of Plasma Physics vol. 7, ed M.A. Leontovich (New York: Consultants Bureau), p. 257 (1979)

[6] D. Palumbo, Some considerations on closed configurations of magnetohydrostatic equilibrium, Nuovo Cimento B **X53**, 507 (1968)

[7] J. Nührenberg, Development of quasi-isodynamic stellarators, Plasma Phys. Contr. Fusion **52**, 124003 (2010)

[8] J. Nührenberg and R. Zille, Stable stellarators with medium β and aspect ratio, Phys. Lett A **114**, 129 (1986)

[9] A.A. Galeev, Diffusion-electrical phenomena in a plasma confined in a tokamak machine, Zh. Eksp. Teor. Fiz. **59**, 1378 (1970) [Sov. Phys. JETP **32**, 752 (1971)]

[10] R.J. Bickerton, J. W. Connor and J. B. Taylor, Diffusion driven plasma currents and bootstrap tokamak, Nature (London) Phys. Sci. **229**, 110 (1971)

[11] M. C. Zarnstorff, M. G. Bell, M. Bitter, R. J. Goldston, B. Grek, R. J. Hawryluk, K. Hill, D. Johnson, D. McCune, H. Park, A. Ramsey, G. Taylor and R. Wieland, Bootstrap current in TFTR, Phys. Rev. Lett. **60**, 1306 (1988)

[12] M. Murakami, B. A. Carreras, L. R. Baylor, G. L. Bell, T. S. Bigelow, A. C. England, J. C. Glowienka, H. C. Howe, T. C. Jernigan, D. K. Lee, V. E. Lynch, C. H. Ma, D. A. Rasmussen, J. S. Tolliver, M. R. Wade, J. B. Wilgen and W. R. Wing, Bootstrap-current experiments in a toroidal plasma-confinement device, Phys. Rev. Lett. **66**, 707 (1991)

[13] P. Helander and J. Nührenberg, Bootstrap current and neoclassical transport in quasi-isodynamic stellarators, Plasma Phys. Contr. Fusion **51**, 055004 (2009)

[14] M. Landreman and P.J. Catto, Omnigenity as generalized quasisymmetry, Phys. Plasmas **19**, 056103 (2012)

[15] M. Hirsch, J. Baldzuhn, C. Beidler, R. Brakel, R. Burhenn, A. Dinklage, H. Ehmler, M. Endler, V. Erckmann, Y. Feng, J. Geiger, L. Giannone, G. Grieger, P. Grigull, H.-J. Hartfuß, D. Hartmann, R. Jaenicke, R. König, H. P. Laqua, H. Maaßberg, K. McCormick, F. Sardei, E. Speth, U. Stroth, F. Wagner,

A. Weller, A. Werner, H. Wobig, S. Zoletnik and for the W7-AS Team, Major results from the stellarator Wendelstein 7-AS, Plasma Phys. Contr. **50**, 053001 (2008)

[16] H. Wobig and S. Rehker, A stellarator coil system without helical windings, in Proceedings of 7th Symposium on Fusion Technology (Grenoble, France), Luxembourg: CID of the CEC, October 24–27, 1972, pp. 333–343.

[17] T. Sunn Pedersen, M. Otte, S. Lazerson, P. Helander, S. Bozhenkov, C. Biedermann, T. Klinger, R. C. Wolf, H. -S. Bosch and The W7-X Team, Confirmation of the topology of the Wendelstein 7-X magnetic field to better than 1:100,000, Nature Comm. **7**, 13493 (2016)

[18] S.A. Bozhenkov, M. Jakubowski, H. Niemann, S.A. Lazerson, G.A. Wurden, C. Biedermann, G. Kocsis, R. König, F. Pisano, L. Stephey, T. Szepesi, U. Wenzel, T. Sunn Pedersen and R.C. Wolf, Effect of error field correction coils on W7-X limiter loads, Nucl. Fusion, at press: https://doi.org/10.1088/1741-4326/aa85ce (2017)

[19] T. Sunn Pedersen, T. Andreeva, H.-S. Bosch, S. Bozhenkov, F. Effenberg, M. Endler, Y. Feng, D.A. Gates, J. Geiger, D. Hartmann, H. Hölbe, M. Jakubowski, R. König, H.P. Laqua, S. Lazerson, M. Otte, M. Preynas, O. Schmitz, T. Stange, Y. Turkin and the W7-X Team, Plans for the first plasma operation of Wendelstein 7-X , Nucl. Fusion **55,** 126001 (2015)

[20] T. Klinger, A. Alonso, S. Bozhenkov, R. Burhenn, A. Dinklage, G. Fuchert, J. Geiger, O. Grulke, A. Langenberg, M. Hirsch, G. Kocsis, J. Knauer, A. Krämer-Flecken, H.P. Laqua, S. Lazerson, M. Landreman, H. Maaßberg, S. Marsen, M. Otte, N. Pablant, E. Pasch, K. Rahbarnia, T. Stange, T. Szepesi, H. Thomsen, P. Traverso, J.L. Velasco, T. Wauters, G. Weir, T. Windisch and the W7-X Team, Performance and properties of the first plasmas of Wendelstein 7-X, Plasma Phys. Contr. Fusion **59**, 014018 (2017)

[21] R.C. Wolf, A. Ali, A. Alonso, J. Baldzuhn, C. Beidler, M. Beurskens, C. Biedermann, H.-S. Bosch, S. Bozhenkov, R. Brakel, A. Dinklage, Y. Feng, G. Fuchert, J. Geiger, O. Grulke, P. Helander, M. Hirsch, U. Höfel, M. Jakubowski, J. Knauer, G. Kocsis, R. König, P. Kornejew, A. Krämer-Flecken, M. Krychowiak, M. Landreman, A. Langenberg, H.P. Laqua, S. Lazerson, H. Maaßberg, S. Marsen, M. Marushchenko, D. Moseev, H. Niemann, N. Pablant, E. Pasch, K. Rahbarnia, G. Schlisio, T. Stange, T. Sunn Pedersen, J. Svensson, T. Szepesi, H. Trimino Mora, Y. Turkin, T. Wauters, G. Weir, U. Wenzel, T. Windisch, G. Wurden, D. Zhang, I. Abramovic, S. Äkäslompolo, P. Aleynikov, K. Aleynikova, R. Alzbutas, G. Anda, T. Andreeva, E. Ascasibar, J. Assmann, S.-G. Baek, M. Banduch, T. Barbui, M. Barlak, K. Baumann, W. Behr, A. Benndorf, O. Bertuch, W. Biel, D. Birus, B. Blackwell, E. Blanco, M. Blatzheim, T. Bluhm, D. Böckenhoff, P. Bolgert, M. Borchardt, V. Borsuk, J. Boscary, L.-G. Böttger, H. Brand, Ch. Brandt, T. Bräuer, H. Braune, S. Brezinsek, K.-J. Brunner, B. Brünner, R. Burhenn, B. Buttenschön, V. Bykov, I. Calvo, B. Cannas, A. Cappa, A. Carls, L. Carraro, B. Carvalho, F. Castejon, A. Charl, F. Chernyshev, M. Cianciosa, R. Citarella, Ł. Ciupiński, G. Claps, M. Cole, M.J. Cole, F. Cordella, G. Cseh, A. Czarnecka, A. Czermak, K. Czerski, M. Czerwinski, G. Czymek, A. da Molin, A. da Silva, G. Dammertz, J. Danielson, A. de la Pena, S. Degenkolbe, P. Denner, D.P. Dhard, M. Dostal, M. Drevlak, P. Drewelow, Ph. Drews, A. Dudek, G. Dundulis, F. Durodie, P. van Eeten, F. Effenberg, G. Ehrke, M. Endler, D. Ennis, E. Erckmann, H. Esteban, T. Estrada, N. Fahrenkamp, J.-H. Feist, J. Fellinger, H. Fernandes, W.H. Fietz, W. Figacz, J. Fontdecaba, O. Ford, T. Fornal, H. Frerichs, A. Freund, M. Führer, T. Funaba, A. Galkowski, G. Gantenbein, Y. Gao, J. García Regaña, M. Garcia-Munoz, D. Gates, G. Gawlik, B. Geiger, V. Giannella, N. Gierse, A. Gogoleva, B. Goncalves, A. Goriaev, D. Gradic, M. Grahl, J. Green, A. Grosman, H. Grote, M. Gruca, C. Guerard, L. Haiduk, X. Han, F. Harberts, J.H. Harris, H.-J. Hartfuß, D. Hartmann, D. Hathiramani, B. Hein, B. Heinemann, P. Heitzenroeder, S. Henneberg, C. Hennig, J. Hernandez Sanchez, C. Hidalgo, H. Hölbe, K.P. Hollfeld, A. Hölting, D. Höschen, M. Houry, J. Howard, X. Huang, M. Huber, V. Huber, H. Hunger, K. Ida, T. Ilkei, S. Illy, B. Israeli, A. Ivanov, S. Jablonski, J. Jagielski, J. Jelonnek, H. Jenzsch, P. Junghans, J. Kacmarczyk, T. Kaliatka, J.-P. Kallmeyer, U. Kamionka, R.

Karalevicius, H. Kasahara, W. Kasparek, N. Kenmochi, M. Keunecke, A. Khilchenko, D. Kinna, R. Kleiber, T. Klinger, M. Knaup, Th. Kobarg, F. Köchl, Y. Kolesnichenko, A. Könies, M. Köppen, J. Koshurinov, R. Koslowski, F. Köster, R. Koziol, M. Krämer, R. Krampitz, P. Kraszewsk, N. Krawczyk, T. Kremeyer, Th. Krings, J. Krom, G. Krzesinski, I. Ksiazek, M. Kubkowska, G. Kühner, T. Kurki-Suonio, S. Kwak, R. Lang, S. Langish, H. Laqua, R. Laube, C. Lechte, M. Lennartz, W. Leonhardt, L. Lewerentz, Y. Liang, Ch. Linsmeier, S. Liu, J.-F. Lobsien, D. Loesser, J. Loizu Cisquella, J. Lore, A. Lorenz, M. Losert, L. Lubyako, A. Lücke, A. Lumsdaine, V. Lutsenko, J. Majano-Brown, O. Marchuk, M. Mardenfeld, P. Marek, S. Massidda, S. Masuzaki, D. Maurer, K. McCarthy, P. McNeely, A. Meier, D. Mellein, B. Mendelevitch, Ph. Mertens, D. Mikkelsen, O. Mishchenko, B. Missal, J. Mittelstaedt, T. Mizuuchi, A. Mollen, V. Moncada, T. Mönnich, T. Morizaki, R. Munk, S. Murakami, F. Musielok, G. Náfrádi, M. Nagel, D. Naujoks, H. Neilson, O. Neubauer, U. Neuner, T. Ngo, R. Nocentini, C. Nührenberg, J. Nührenberg, S. Obermayer, G. Offermanns, K. Ogawa, J. Ongena, J.W. Oosterbeek, G. Orozco, M. Otte, L. Pacios Rodriguez, W. Pan, N. Panadero, N. Panadero Alvarez, A. Panin, D. Papenfuß, S. Paqay, A. Pavone, E. Pawelec, G. Pelka, X. Peng, V. Perseo, B. Peterson, A. Pieper, D. Pilopp, S. Pingel, F. Pisano, B. Plaum, G. Plunk, M. Povilaitis, J. Preinhaelter, J. Proll, M.-E. Puiatti, A. Puig Sitjes, F. Purps, M. Rack, S. Récsei, A. Reiman, D. Reiter, F. Remppel, S. Renard, R. Riedl, J. Riemann, S. Rimkevicius, K. Riße, A. Rodatos, H. Röhlinger, M. Romé, P. Rong, H.-J. Roscher, B. Roth, L. Rudischhauser, K. Rummel, T. Rummel, A. Runov, N. Rust, L. Ryc, S. Ryosuke, R. Sakamoto, A. Samartsev, M. Sanchez, F. Sano, S. Satake, G. Satheeswaran, J. Schacht, F. Schauer, T. Scherer, A. Schlaich, K.-H. Schlüter, J. Schmitt, H. Schmitz, O. Schmitz, S. Schmuck, M. Schneider, W. Schneider, M. Scholz, P. Scholz, R. Schrittwieser, M. Schröder, T. Schröder, R. Schroeder, H. Schumacher, B. Schweer, B. Shanahan, I.V. Shikhovtsev, M. Sibilia, P. Sinha, S. Sipliä, J. Skodzik, C. Slaby, H. Smith, W. Spiess, D.A. Spong, A. Spring, R. Stadler, B. Standley, L. Stephey, M. Stoneking, U. Stridde, Z. Sulek, C. Surko, Y. Suzuki, V. Szabó, T. Szabolics, Z. Szőkefalvi-Nagy, N. Tamura, A. Terra, J. Terry, J. Thomas, H. Thomsen, M. Thumm, C.P. von Thun, D. Timmermann, P. Titus, K. Toi, J.M. Travere, P. Traverso, J. Tretter, H. Tsuchiya, T. Tsujimura, S. Tulipán, M. Turnyanskiy, B. Unterberg, J. Urban, E. Urbonavicius, I. Vakulchyk, S. Valet, B. van Millingen, L. Vela, J.-L. Velasco, M. Vergote, M. Vervier, N. Vianello, H. Viebke, R. Vilbrandt, A. Vorkörper, S. Wadle, F. Wagner, E. Wang, N. Wang, F. Warmer, L. Wegener, J. Weggen, Y. Wei, J. Wendorf, A. Werner, B. Wiegel, F. Wilde, E. Winkler, V. Winters, S. Wolf, J. Wolowski, A. Wright, P. Xanthopoulos, H. Yamada, I. Yamada, R. Yasuhara, M. Yokoyama, J. Zajac, M. Zarnstorff, A. Zeitler, H. Zhang, J. Zhu, M. Zilker, A. Zimbal, A. Zocco, S. Zoletnik and M. Zuin, Major results from the first plasma campaign of the Wendelstein 7-X stellarator, Nucl. Fusion **57,** 102020 (2017)

[22] T. Sunn Pedersen, A. Dinklage, Yu. Turkin, R. Wolf, S.A. Bozhenkov, J. Geiger, G. Fuchert, H.-S. Bosch, K. Rahbarnia, H. Thomsen, U. Neuner, T. Klinger, A. Langenberg, H. Trimiño Mora, P. Kornejew, J. Knauer, M. Hirsch, the W7-X Team and N. Pablant, Key results from the first plasma operation phase and outlook for future performance in Wendelstein 7-X, Phys. Plasmas **24**, 055503 (2017)

[23] R.C. Wolf, C. D. Beidler, A. Dinklage, P. Helander, H. P. Laqua, F. Schauer, T. Sunn Pedersen, F. Warmer and W7-X Team, Wendelstein 7-X Program—Demonstration of a Stellarator Option for Fusion Energy, IEEE Trans. Act. Plasma Sci. **44**, 1466 (2016)

[24] G.A. Wurden, C. Biedermann, F. Effenberg, M. Jakubowski, H. Niemann, L. Stephey, S. Bozhenkov, S. Brezinsek, J. Fellinger, B. Cannas, F. Pisano, S. Marsen, H.P. Laqua, R. König, O. Schmitz, J.H. Harris, E.A. Unterberg and the W7-X Team, Limiter observations during W7-X first plasmas, *Nucl. Fusion* **57** 056036 (2017)

[25] M . Endler, B. Brucker, V. Bykov, A. Cardella, A. Carls, F. Dobmeier, A. Dudek, J. Fellinger, J. Geiger, K. Grosser, O. Grulke, D. Hartmann, D. Hathiramani, K. Höchel, M. Köppen, R. Laube, U.

Neuner, X. Peng, K. Rahbarnia, K. Rummel, T. Sieber, S. Thiel, A. Vorköper, A. Werner, T. Windisch, M.Y. Ye, Engineering design for the magnetic diagnostics of Wendelstein 7-X, Fusion Eng. Design **100**, 468 (2015)

[26] K. Rahbarnia, T. Andreeva, A. Cardella, B.B. Carvalho, M. Endler, D. Hathiramani, J. Geiger, O. Grulke, S. Lazerson, U. Neuner, J. Svensson, H. Thomsen, A. Werner and W7-X Team, Commissioning of the magnetic diagnostics during the first operation phase at Wendelstein 7-X, 43rd EPS Conference on Plasma Physics, P4.011, Europhys. Conf. Abstr. **40A**, Eds. P. Mantica, G. Giruzzi, M. Fajardo, T. Gans, S. Poedts, N. Vennekens, European Physical Society, Mulhouse, France, 2016; K. Rahbarnia et al., to be submitted.

[27] H. Yamada, J.H. Harris, A. Dinklage, E. Ascasibar, F. Sano, S. Okamura, J. Talmadge, U. Stroth, A. Kus, S. Murakami, M. Yokoyama, C.D. Beidler, V. Tribaldos, K.Y. Watanabe and Y. Suzuki, Characterization of energy confinement in net-current free plasmas using the extended International Stellarator Database, Nucl. Fusion **45**, 1684 (2005)

[28] U. Stroth, M. Murakami, R.A. Dory, H. Yamada, S. Okamura, F. Sano and T. Obiki , Energy confinement scaling from the international stellarator database, Nucl. Fusion **36**, 1063 (1996)

[29] A. Dinklage, H. Maaßberg, R. Preuss, Yu.A. Turkin, H. Yamada, E. Ascasibar, C.D. Beidler, H. Funaba, J.H. Harris, A. Kus, S. Murakami, S. Okamura, F. Sano, U. Stroth, Y. Suzuki, J. Talmadge, V. Tribaldos, K.Y. Watanabe, A. Werner, A. Weller and M. Yokoyama, Physics model assessment of the energy confinement time scaling in stellarators, Nucl. Fusion **47**, 1265 (2007)

[30] M. Hirsch, A. Dinklage, A. Alonso, G. Fuchert, S. Bozhenkov, U. Höfel, T. Andreeva, J. Baldzuhn, M. Beurskens, H.-S. Bosch, C.D. Beidler, C. Biedermann, E. Blanco, R. Brakel, R. Burhenn, B. Buttenschön, A. Cappa, A. Czarnecka, M. Endler, T. Estrada, T. Fornal, J. Geiger, O. Grulke, J.H. Harris, D. Hartmann, M. Jakubowski, T. Klinger, J. Knauer, G. Kocsis, R. König, P. Kornejew, A. Krämer-Flecken, N. Krawczyk, M. Krychowiak, M. Kubkowska, I. Ksiazek, A. Langenberg, H.P. Laqua, S. Lazerson, H. Maaßberg, N. Marushchenko, S. Marsen, V. Moncada, D. Moseev, D. Naujoks, M. Otte, N. Pablant, E. Pasch, F. Pisano, K. Rahbarnia, T. Schröder, T. Stange, L. Stephey, T. Szepesi, T. Sunn Pedersen, H. Trimino Mora, H. Thomsen, H. Tsuchiya, Yu. Turkin, T. Wauters, G. Weir, U. Wenzel, A. Werner, R. Wolf, G.A. Wurden, D. Zhang and the W7-X Team, Confinement in Wendelstein 7-X limiter Plasmas, Nucl. Fusion **57**, 086010 (2017)

[31] E.J. Doyle, W.A. Houlberg, Y. Kamada, V. Mukhovatov, T.H. Osborne, A. Polevoi, G. Bateman, J.W. Connor, J.G. Cordey, T. Fujita, X. Garbet, T.S. Hahm, L.D. Horton, A.E. Hubbard, F. Imbeaux, F.Jenko, J.E. Kinsey, Y. Kishimoto, J. Li, T.C. Luce, Y. Martin, M. Ossipenko, V. Parail, A. Peeters, T.L. Rhodes, J.E. Rice, C.M. Roach, V. Rozhansky, F. Ryter, G. Saibene, R. Sartori, A.C.C. Sips, J.A. Snipes, M. Sugihara, E.J. Synakowski, H. Takenaga, T. Takizuka, K. Thomsen, M.R. Wade, H.R. Wilson, Chapter 2: Plasma confinement and Transport, Nucl Fusion **48**, 099801 (2008)

[32] Yu. Turkin, H. Maaßberg, C.D. Beidler, J. Geiger, and N. Marushchenko, Current control by ECCD for W7-X, Fusion Sci. Technol. **50** , 10.13182 (2006)

[33] Yu. Turkin, C. D. Beidler, H. Maaßberg, S. Murakami, V. Tribaldos, A. Wakasa, Neoclassical transport simulations for stellarators, Phys. Plasmas **18**, 022505 (2011)

[34] A. Langenberg, N.A. Pablant, O. Marchuk, D. Zhang, J.A. Alonso, R. Burhenn, J. Svensson, P. Valson, D. Gates, M. Beurskens, R.C. Wolf and the W7-X Team, Argon impurity transport studies at Wendelstein 7-X using x-ray imaging spectrometer measurements, Nucl. Fusion **57**, 086013 (2017)

[35] A. Kraemer-Flecken, T. Windisch, W. Behr, G. Czymek, P. Drews, G. Fuchert, J. Geiger, O. Grulke, M. Hirsch, M. Knaup, Y. Liang, O. Neubauer, E. Pasch, J. Velasco, W7X-Team, Investigation of

turbulence rotation in limiter plasmas at W7-X with a new installed poloidal correlation reflectometry, Nucl. Fusion **57**, 066023 (2017)

[36] H.-S. Bosch, R. Brakel, T. Braeuer, V. Bykov, P. van Eeten, J.-H. Feist, F. Füllenbach, M. Gasparotto, H. Grote, T. Klinger, H. Laqua, M. Nagel, D. Naujoks, M. Otte, K. Risse, T. Rummel, J. Schacht, A. Spring, T. Sunn Pedersen, R. Vilbrandt, L. Wegener, A. Werner, R.C. Wolf, J. Baldzuhn, C. Biedermann, H. Braune, R. Burhenn, M. Hirsch, U. Höfel, J. Knauer, P. Kornejew, S. Marsen, T. Stange, H. Trimino Mora and W7-X Team, Final integration, commissioning and start of the Wendelstein 7-X stellarator operation , Nucl. Fusion **57**, 116015 (2017)

[37] S. Marsen, Y. Corre, H.P. Laqua, V. Moncada, D. Moseev, H. Niemann, M. Preynas, T. Stange and The W7-X Team, First results from protective ECRH diagnostics for Wendelstein 7-X, Nucl. Fusion **57**, 086014 (2017)

[38] D. Moseev, H.P. Laqua, S. Marsen, N. Marushchenko, T. Stange, H. Braune, F. Gellert, M. Hirsch, U. Hoefel, J. Knauer, J.W. Oosterbeek, Y. Turkin and the W7-X Team, Inference of the microwave absorption coefficient from stray radiation measurements in Wendelstein 7-X, Nucl. Fusion **57**, 036013 (2017)

[39] C.D. Beidler, K. Allmaier, M.Yu. Isaev, S.V. Kasilov, W. Kernbichler, G.O. Leitold, H. Maaßberg, D.R. Mikkelsen, S. Murakami, M. Schmidt, D.A. Spong, V. Tribaldos and A. Wakasa, Benchmarking of the mono-energetic transport coefficients—results from the International Collaboration on Neoclassical Transport in Stellarators (ICNTS), Nucl. Fusion **51**, 076001 (2011)

[40] C. Beidler, G. Grieger, F. Herrnegger, E. Harmeyer, J. Kisslinger, W. Lotz, H. Maassberg, P. Merkel, J. Nührenberg, F. Rau, J. Sapper, F. Sardei, R. Scardovelli, A. Schlüter and H. Wobig, Physics and Engineering Design for Wendelstein VII-X, Fusion Technol. **17**, 148 (1990)

[41] S.P. Hirshman, W.I. van Rij and P. Merkel, Three-dimensional free boundary calculations using a spectral Green's function method, Comput. Phys. Commun. **43**, 143 (1986)

[42] S.A. Bozhenkov, J. Geiger, M. Grahl, J. Kißlinger, A. Werner, R.C. Wolf, Service oriented architecture for scientific analysis at W7-X. An example of a field line Tracer, Fusion Eng. Des**. 88**, 2997 (2013)

[43] S.P. Hirshman, K. C. Shaing, W. I. van Rij, and E. C. Crume Jr., Plasma transport coefficients for nonsymmetric toroidal confinement systems, Physics of Fluids **29**, 2951 (1986)

[44] W.I. van Rij and S.P. Hirshman, Variational bounds for transport coefficients in three-dimensional toroidal plasmas , Phys. Fluids B **1**, 563 (1989)

[45] M. Landreman, H. M. Smith, A. Mollén, and P. Helander, Comparison of particle trajectories and collision operators for collisional transport in nonaxisymmetric plasmas, Phys. Plasmas **21**, 042503 (2014)

[46] N. Marushchenko, Yu. Turkin, H. Maaßberg, Ray-tracing code TRAVIS for ECR heating, EC current drive and ECE diagnostic, Comp. Phys. Comm. **185**, 165 (2014)

[47] Y. Feng, F. Sardei, J. Kisslinger, P. Grigull, K. Mc Cormick, D. Reiter, 3D Edge Modeling and Island Divertor Physics, Contrib. Plasma Phys. **44**, 57 (2004)

[48] F. Effenberg, Y. Feng, O. Schmitz, H. Frerichs, S.A. Bozhenkov, H. Hölbe, R. König, M. Krychowiak, T. Sunn Pedersen, D. Reiter, L. Stephey and W7-X Team, Numerical investigation of plasma edge transport and limiter heat fluxes in Wendelstein 7-X startup plasmas with EMC3-EIRENE , Nucl. Fusion **57,** 036021 (2017)

[49] M. Krychowiak, A. Adnan, A. Alonso, T. Andreeva, J. Baldzuhn, T. Barbui, M. Beurskens, W. Biel, C. Biedermann, B. D. Blackwell, H. S. Bosch, S. Bozhenkov, R. Brakel, T. Bräuer, B. Brotas de Carvalho, R. Burhenn, B. Buttenschön, A. Cappa, G. Cseh, A. Czarnecka, A. Dinklage, P. Drews, A. Dzikowicka, F. Effenberg, M. Endler, V. Erckmann, T. Estrada, O. Ford, T. Fornal, H. Frerichs, G. Fuchert, J. Geiger, O. Grulke, J. H. Harris, H. J. Hartfuß, D. Hartmann, D. Hathiramani, M. Hirsch, U. Höfel, S. Jabłoński, M. W. Jakubowski, J. Kaczmarczyk, T. Klinger, S. Klose, J. Knauer, G. Kocsis, R. König, P. Kornejew, A. Krämer-Flecken, N. Krawczyk, T. Kremeyer, I. Książek, M. Kubkowska, A. Langenberg, H. P. Laqua, M. Laux, S. Lazerson, Y. Liang, S. C. Liu, A. Lorenz, A. O. Marchuk, S. Marsen, V. Moncada, D. Naujoks, H. Neilson, O. Neubauer, U. Neuner, H. Niemann, J. W. Oosterbeek, M. Otte, N. Pablant, E. Pasch, T. Sunn Pedersen, F. Pisano, K. Rahbarnia, L. Ryć, O. Schmitz, S. Schmuck, W. Schneider, T. Schröder, H. Schuhmacher, B. Schweer, B. Standley, T. Stange, L. Stephey, J. Svensson, T. Szabolics, T. Szepesi, H. Thomsen, J.-M. Travere, H. Trimino Mora, H. Tsuchiya, G. M. Weir, U. Wenzel, A. Werner, B. Wiegel, T. Windisch, R. Wolf, G. A. Wurden, D. Zhang, A. Zimbal and W7-X Team , Overview of diagnostic performance and results for the first operation phase in Wendelstein 7-X, Rev. Sci. Instrum. **87**, 11D304 (2016)

[50] N.A. Pablant, A. Langenberg, A. Alonso, C.D. Beidler, M. Bitter, S. Bozhenkov, R. Burhenn, M. Beurskens, L. Delgado-Aparicio, A. Dinklage, G. Fuchert, D. Gates, J. Geiger, K.W. Hill, U. Hoefel, M. Hirsch, J. Knauer, A. Krämer-Flecken, M. Landreman, S. Lazerson, H. Maassberg, O. Marchuk, S. Massidda, G.H. Neilson, E. Pasch, S. Satake, J. Svennson, P. Traverso, Y. Turkin, P. Valson, J.L. Velasco, G. Weir, T. Windisch, R.C. Wolf, M. Yokoyama, D. Zhang, and the W7-X Team, Core Radial Electric Field and Transport in Wendelstein 7-X Plasmas, submitted to Phys. Plasmas

[51] M.Romé, V. Erckmann, U. Gasparino, N. Karulin, Electron cyclotron resonance heating and current drive in the W7-X stellarator, Plasma Phys. Contr. Fusion **40**, 511 (1998)